Environ. Sci. Technol. **2006**, *40,* 5015−5021

Observed and Simulated Fluid Drag Effects on Colloid Deposition in the Presence of an Energy Barrier in an Impinging Jet System

WILLIAM P. JOHNSON* AND MEIPING TONG

Department of Geology and Geophysics, University of Utah, Salt Lake City, Utah 84112

The deposition and re-entrainment behaviors of carboxylate-modified latex microspheres (0.2-, 0.5-, 1.0-, and 2.0-μm diameter) were examined in an impinging jet system on both glass and quartz substrata under a variety of environmentally relevant fluid velocities (2.12×10^{-4} to 1.06×10^{-3} m sec^{-1}) in both the absence and the presence of an energy barrier to deposition. In the absence of an energy barrier to deposition, deposition fluxes onto glass and quartz substrata increased with increasing fluid velocity for all four microsphere sizes, in accordance with expectations from theory. In contrast, in the presence of an energy barrier to deposition, deposition efficiencies onto glass and quartz substrata decreased with increasing fluid velocity for all four microsphere sizes. Lack of re-entrainment and observed strong attachment were consistent with the expectation that deposition occurs via the primary energy minima where nanoscale surface heterogeneity locally reduces or eliminates the energy barrier to deposition. Colloid deposition onto an overall opposite-charged surface was simulated using a particle transport model with randomly distributed hetero domains that were like-charged relative to the colloid. Varying the size and number of the hetero domains showed that simulated colloid deposition efficiencies decreased with increasing fluid velocity when the hetero domains were small relative to the colloid. The simulations thereby demonstrate that observed decreases in colloid deposition efficiencies with increasing fluid velocity are consistent with the hypothesis that colloid deposition onto overall like-charged surfaces occurs at nanoscale hetero domains where repulsion is locally reduced or eliminated.

Introduction

The rate at which colloids deposit onto grain surfaces during transport through porous media depends on physical and chemical characteristics of the system, and can be quantified via a deposition rate coefficient (k_f), which is proportional to the product of the probability of colloid collision with the grain surfaces (η), and the probability of colloid attachment upon collision (α)

$$k_f = \frac{3}{2}\frac{(1-\theta)}{d_c}\alpha\eta v \quad (1)$$

where θ is the sediment porosity, d_c is the collector (porous media grain) diameter, and v is the fluid velocity. The equations comprising the single collector efficiency (η) predict the rate of collision of colloids with grain surfaces during transport in porous media due to advection on surface-intercepting streamlines, and colloid crossover to intercepting streamlines via diffusion and gravitational settling (*1*−*4*). Hence, the parameter η incorporates known physical mass transfer processes that lead to collision. Under conditions absent a repulsive energy barrier, the correlation equations for η reasonably predict the deposition rate coefficient (k_f), and the predicted and observed k_f increases with increasing fluid velocity in porous media (*5*−*7*).

The value of k_f is also governed by the overall interaction energy between the colloid and the surface, which is a function of their separation distance, and which is comprised (classically) of two interactions: van der Waals and electric double layer interactions (*8*−*11*). The electric double layer interaction energy is repulsive when the colloid and the grain surfaces are like-charged, and the distance over which this repulsion extends is inversely related to solution ionic strength (*12, 13*). In contrast, the van der Waals interaction is attractive for the vast majority of surfaces, and is considered to be independent of solution chemistry (*14, 15*). These two classic interactions decay with colloid−surface separation distance at distinct rates, such that van der Waals attraction may greatly dominate at small separation distances (primary energy minimum), electric double layer repulsion may dominate at intermediate separation distances (energy barrier to attachment), and van der Waals attraction may slightly dominate at greater separation distances (secondary energy minimum). The energy barrier to deposition is absent when the colloid and grain surfaces are oppositely charged, or when the ionic strength is sufficiently high to compress the electric double layer repulsion to short separation distances.

Under equivalent physical conditions, the value of k_f is lower in the presence relative to the absence of an energy barrier to deposition, and the ratio of k_f in the presence versus the absence of an energy barrier to deposition is called the deposition efficiency (α), where α is less than or equal to unity. Although a great deal of colloid transport research has demonstrated the expected qualitative inverse relationship between the magnitude of α and the height of the energy barrier to deposition; quantitative prediction of α has not been attained. Measured bulk surface characteristics, e.g., zeta potentials via electrophoretic mobilities or streaming potentials, are too coarse to reflect fine-scale surface characteristics that govern colloid deposition (*16*). For example, deposition is observed even when measured bulk surface characteristics translate to significant repulsive colloid−surface interactions that should prevent deposition (*17*).

The inability of existing theory to predict α in the presence of an energy barrier to deposition has spawned a body of research demonstrating that surface roughness may decrease repulsive colloid−surface interaction (*18, 19*), and that surface charge heterogeneity locally eliminates repulsive colloid−surface interaction (*20*−*23*). Although characterization of roughness and surface charge heterogeneity is extremely challenging, the existence of heterogeneous domains of various scales on surfaces is supported by a variety of observations, as reviewed by Zembala (*24*).

* Corresponding author phone: (801) 581-5033; fax: (801) 581-7065; e-mail: wjohnson@earth.utah.edu.

10.1021/es060450c CCC: $33.50 © 2006 American Chemical Society
Published on Web 07/14/2006

Classic filtration theory provides an excellent match between predicted and observed values of k_f in the absence of an energy barrier to deposition. However, in the presence of an energy barrier to deposition, compiled data demonstrate that colloid deposition efficiencies (α) in porous media decrease with increasing fluid velocity for a variety of colloid types (viruses, bacteria, carboxylate-modified latex microspheres) and sizes (e.g., 50-nm to 5.7-μm diameters) (*25*). That α decreases with increasing fluid velocity in bulk repulsive media implicates fluid drag as a mitigating influence on colloid deposition in porous media.

Fluid drag influences in porous media are complicated by the fact that grain to grain contacts and rear stagnation points in porous media yield complex fluid flow fields. For this reason, comparative colloid deposition experiments can be run in impinging jet systems, where the fluid is directed normal to a flat surface (the system lacks grain to grain contacts and rear stagnation points). The impinging jet system reflects deposition onto the forward stagnation points of porous media grains. If observed values of α in the impinging jet decrease with increasing fluid velocity, then it is reasonable to conclude that the mechanism mitigating colloid deposition in the presence of an energy barrier in the impinging jet operates also (but perhaps not exclusively) in porous media under equivalent conditions. Recent experiments in an impinging jet system indicated that α decreased with increasing fluid velocity in the presence of an energy barrier to deposition (*26*); however, this trend was demonstrated only for a single microsphere size (1-μm diameter), since no deposition was observed for the other microsphere size examined (5.7-μm diameter) under the relatively high fluid velocities of the experiments.

The objective of this paper is to demonstrate for a range of colloid sizes (0.2- to 2.0-μm diameter), two impinging surfaces (quartz and glass), and three fluid velocities representing forced groundwater gradients and engineered filtration systems, that deposition fluxes increased with increasing fluid velocity when an energy barrier to deposition was absent, whereas α values decreased with increasing fluid velocity when an energy barrier to deposition was present. These observations indicate a mitigating effect of fluid drag on colloid deposition in the presence of an energy barrier for these circum-μm colloids in this fluid velocity regime. Simulations are presented using a particle transport model that incorporates forces acting on the colloids (electric double layer, van der Waals, gravity, diffusion, and fluid drag) and where deposition onto overall like-charged surfaces occurs via randomly distributed localized zones of attraction (hetero domains). The simulations indicate that the observed decreases in α with increasing fluid velocity can be expected when the hetero domains are small relative to the colloid, due to the decreased probability of colloid interception with the hetero domains.

Materials and Methods

Microsphere Preparation. Spherical fluorescent carboxylate-modified polystyrene latex microspheres (Molecular Probes, Inc., Eugene, OR) of four sizes (0.2-, 0.5-, 1.0-, and 2.0-μm) were used in all experiments, except as noted. The vendor-supplied surface charge densities were 0.282, 0.1419, 0.0175, and 0.1076 meq g^{-1} respectively. The vendor-supplied stock particle concentrations of the 0.2-, 0.5-, 1.0-, and 2.0-μm microspheres were 4.5×10^{12}, 2.9×10^{11}, 2.7×10^{10}, and 4.5×10^{9} microspheres mL^{-1}, respectively. All stock solutions contained NaN_3 (2 mM). In addition, the 2.0-μm microsphere stock suspension contained 0.01% Tween-20.

Prior to injection, stock solutions for the 0.2-, 0.5-, and 1.0-μm microspheres were diluted in NaCl solution to achieve a nominal influent concentration (C_o) of 1.0×10^7 particles mL^{-1} at the desired strength (NaCl) plus MOPS buffer (2.2 mM) yielding a solution pH of 6.72. The stock solution for 2.0-μm microspheres was first diluted 10 times in pure (Milli-Q) water, and was washed three times to remove Tween-20. Washing involved centrifugation (10 000*g* for 10 min at 4 °C), followed by decanting, and addition of pure water. Following washing, the 2.0-μm microsphere solution was diluted in NaCl solution to achieve a nominal influent concentration (C_o) of 1.0×10^6 at the desired ionic strength (NaCl) plus MOPS buffer (2.2 mM), yielding a solution pH of 6.72.

Impinging Jet System. An impinging jet system was utilized for colloid deposition experiments. The microsphere suspension was introduced by a syringe pump (Harvard Appartus, Holliston, MA) into the stainless steel flow cell downward through a 1 mm i.d. stainless steel capillary tube. The transparent glass or quartz substratum was located 1 mm from the inlet capillary tube. Fluid removal from the flow cell occurred via four equally spaced stainless steel capillary tubes (i.d. 0.5 mm), located 12.5 mm from the inlet capillary tube on the upper surface of the flow cell.

Total internal reflection fluorescence microscopy (TIRFM) was used to directly observe deposition of microspheres in impinging jet system. TIRFM exploits the evanescent wave produced at the substratum−solution interface. Since the depth of the evanescent field is restricted to a very short distance from the interface (typically <150 nm), only those particles at, or very close to, the solution−substratum interface are illuminated. The utility of TIRFM (as opposed to bulk fluorescence) is demonstrated in the Supporting Information.

The evanescent wave was produced via a Melles Griot model IMA 101 Argon laser (Melles Griot Laser Group, Carlsbad, CA) tuned to a wavelength of 488 nm. An equilateral prism (15 mm) (Edmund Industrial Optics, Barrington, NJ) placed on the bottom surface of the substratum was used to introduce the laser light at the critical angle (> 57.9°) from the horizon to produce internal reflection in the substratum.

The flow cell was mounted on the microscope stage (Eclipse TE2000-S inverted microscope) (Nikon, Japan). Band-pass filters were used to restrict emission wavelengths to 520 ± 20 nm thereby eliminating blue light scattered from the stainless steel flow cell. A 10× long-distance working objective (Nikon, Japan) was used to magnify the image.

Images of deposited microspheres were recorded by a CCD camera CoolSNAP HQ (Photometrics, Tucson, AZ) and analyzed using the image analysis software Metamorph Meta 6.2R6 (Universal Imaging Corp., Downingtown, PA). The observation area (450 μm × 336 μm) was imaged at regular intervals, e.g., 3 s, where the time interval between images was set to the highest value that produced 2 or less deposition or re-entrainment events between subsequent images.

The number of deposited microspheres was compared between successive images to determine deposition and re-entrainment events by tracking object intensity relative to a specific threshold. The specific threshold was chosen on the basis of eliminating digital noise while retaining all deposited colloids. Size and shape were also used to distinguish digital noise from deposited colloids.

The deposition flux was determined from the slope of the initial (linear) portion of the curve representing the number of deposited microspheres versus time. This slope was divided by the observation area (450 μm × 336 μm) and the influent microsphere concentration. The deposition flux in the presence of an energy barrier to deposition is presented in terms of deposition efficiency, α, which again is the ratio of the deposition flux in the presence of an energy barrier (k_{fp}) relative to that in the absence of an energy barrier (k_{fa}).

$$\alpha = \frac{k_{fp}}{k_{fa}} \tag{2}$$

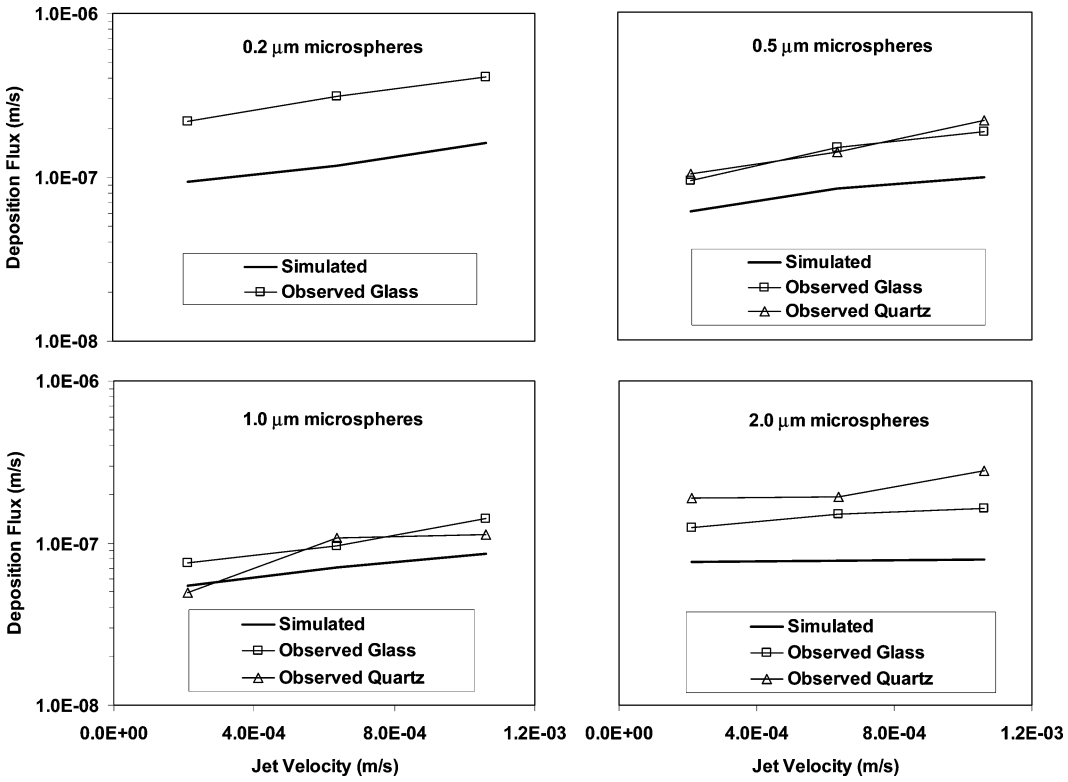

FIGURE 1. Observed and simulated deposition fluxes on glass and quartz for the four sizes of microspheres as a function of fluid velocity in the absence of an energy barrier to deposition.

Substrata Preparation. Glass microscope slides (Fisher Scientific, Inc.) and quartz microscope slides (Electron Microscopy Sciences, Hatfield, PA) of dimension 25 × 75 × 1 mm were used in the impinging jet flow cell. These two surfaces were used in order to determine whether the observations were applicable to multiple materials that are like-charged with respect to the colloid under environmental conditions.

The SC-1 cleaning procedure (*27*) was used for cleaning both the quartz and glass substrata. The procedure involved boiling the substrata in a 5:1:1 solution of deionized water, 30% H_2O_2, and 27% NH_4OH at 75−80 °C for 10 min to remove organic materials and metal oxides from the substrata. Boiling was performed in a Pyrex glass beaker for the glass substratum, whereas boiling was performed in a quartz container for the quartz substratum. Following the SC-1 cleaning process, the substratum was thoroughly rinsed with pure water (Millipore Gradient A10, Millipore Corporation, Billerica, MA), dried with pure compressed N_2 gas (high purity), and placed in the impinging jet flow cell.

Experimental Conditions. The pH of all influent solutions was 6.72 (set by MOPS buffer) except where noted, and flow cell effluents were monitored to ensure pH remained constant (<0.01 pH unit change) during the experiments. Ionic strength of the influent solution was varied in order to produce a range of energy barrier heights corresponding to α ranging from 1 to 0.

Experiments in the presence of an energy barrier to deposition were conducted at an ionic strength of 0.05 M for all microsphere sizes. Experiments performed in the absence of an energy barrier were conducted at various ionic strengths depending on the strategy used to eliminate the energy barrier. For the 1.0-μm microspheres, conditions absent an energy barrier were generated by use of amine-functionalized polystyrene latex microspheres (Molecular Probes, Inc., Eugene, OR) at an ionic strength of 0.001 M. The amine-functionalized microspheres had a stock concentration of 4.5×10^{10} mL^{-1}, a diameter of 0.93 μm, and a surface charge of 0.9176 meq g^{-1}. Since amine-modified microspheres were not commercially available in the 0.2-, 0.5-, and 2.0-μm sizes, elimination of the energy barrier for the 0.2-, 0.5-, and 2.0-μm microspheres was achieved by lowering solution pH to 2 (HCl addition) and increasing the solution ionic strength to 0.05 M (NaCl).

Flow rates were varied from 0.01, 0.03, and 0.05 mL min^{-1}, which correspond to tangential fluid velocities (1 μm from the impinging surface) of 0.016, 0.056, and 0.106 m day^{-1}. In contrast, Brow et al. (*26*) examined conditions where tangential fluid velocities (1 μm from the impinging surface) were significantly higher; ranging from 0.05 to 0.40 m day^{-1}, and where no deposition of the larger microspheres (5.7-μm) was observed in the presence of an energy barrier to deposition. Lower near-surface fluid velocities used here allowed the deposition of the largest microspheres (2.0-μm) and thereby allowed the establishment of trends in deposition efficiencies versus fluid velocity in the presence of an energy barrier to deposition. The corresponding cross-sectionally averaged fluid velocities in the impinging jet ranged from 18.3 to 91.6 m day^{-1}; which represent fluid velocities in coarse aquifer sediments, forced-gradient conditions, or engineered filtration systems. All experiments were carried out at room temperature (22 °C).

Electrokinetic Characterization and Interaction Energies. Electrophoretic mobility measurements of the microspheres were performed using a zeta analyzer (ZetaPALS, Brookhaven Instruments Corporation, Holtsville, NY), at a microsphere concentration of 10^6 particles mL^{-1}. Measurements were performed in NaCl solution with ionic strength ranging from 0.001 to 0.1 M at pH 6.72 and room temperature (22 °C), to reflect experimental conditions. The electrophoretic mobility measurements were repeated 6−12 times. Measurements beyond an ionic strength of 0.1 M were not reproducible due to the low electrophoretic mobility, as well as due to heating of the highly conductive solution in the instrument.

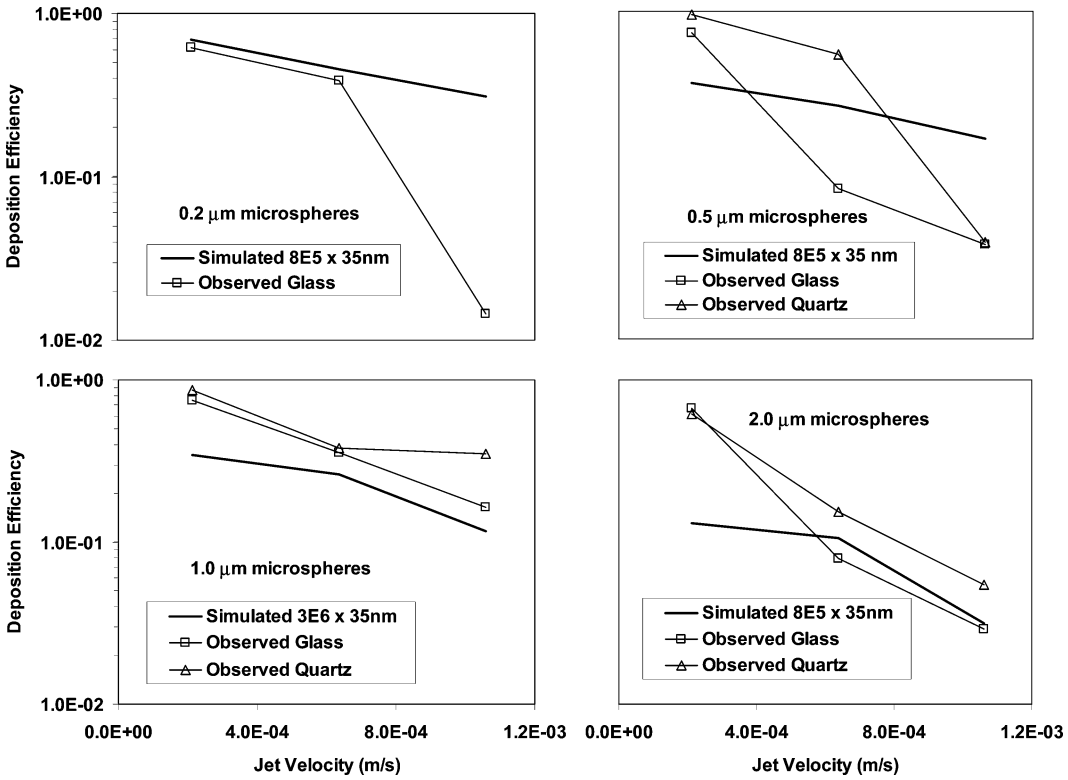

FIGURE 2. Observed and simulated deposition efficiencies on glass and quartz for the four sizes of microspheres as a function of fluid velocity in the presence of an energy barrier to deposition. Simulations were performed using either 8E5 or 3E6 hetero domains that were 35 nm in size.

The electrokinetic properties of the glass substratum were determined by measuring the crushed glass substratum using the zeta analyzer at a particle concentration of 10^6 particles mL^{-1}. The electrokinetic properties of quartz substratum were estimated from values given in Kuznar et al. (*28*).

ζ-Potentials were calculated from the measured electrophoresis mobilities using the von Smoluchowski equation (*29*). The von Smoluchowski formula is based on a surface model in which the electric charges are located at the ideal ion-impenetrable surface of zero thickness. The ζ-potentials of the microspheres and crushed glass substratum as a function of ionic strength and pH are presented in the Supporting Information.

Both the carboxylate-modified microspheres and the glass substratum were negatively charged at pH 6.72, and their ζ-potentials became less negative (near zero) at pH 2 (Supporting Information). ζ-potential of amine-functionalized microspheres was +9.2 mV at an ionic strength of 0.001 M. ζ-potential of both glass and quartz substratum was about −56 mV at an ionic strength of 0.05 M and pH 6.72, whereas this ζ-potential was about −8 mV at an ionic strength of 0.05 M and pH 2 (*28*). The ζ-potentials were used to calculated DLVO interaction energies between the spheres and substratum surfaces.

According to classic DLVO theory, the total interaction energy between a colloid and a surface can be represented by van der Waals and electric double layer interactions. The electric double layer interaction energy was calculated according to Gregory (*30*) (linear superposition approximation), whereas the van der Waals attractive energy (with electromagnetic retardation) was calculated according to Gregory (*15*). The calculated DLVO interaction energy profiles between the microspheres and substrata (glass and quartz), were nearly equivalent for the two substrata, yielding energy barriers to deposition of 102, 423, 1176, and 2655 kT for the 0.2-, 0.5-, 1.0-, and 2.0-μm microspheres, respectively, at an ionic strength 0.05 M and pH of 6.72. In contrast, at pH 2 and an ionic strength of 0.05 M, the energy barrier to deposition was absent for colloid interaction with both surfaces. The interaction energy profiles are described in further detail in the Supporting Information.

Results

Deposition Flux in the Absence of an Energy Barrier to Deposition. Deposition fluxes onto glass and quartz substrata for all four microsphere sizes increased with increasing fluid velocity in the absence of an energy barrier to deposition (Figure 1). The increase in deposition flux with increasing fluid velocity observed in the absence of an energy barrier to deposition is expected based on theoretical considerations, as demonstrated via numerical simulations incorporating all forces expected to act during colloid transport in this system (electric double layer, van der Waals, gravity, diffusion, and fluid drag) (Figure 1). The experimental conditions, numerical model, and simulation results are described in detail in the Supporting Information, and the parameters used in the simulations closely reflected experimental conditions. Zeta potentials of the colloid ($\zeta_p = -60$ mV) and the impinging surface ($\zeta_c = +5$ mV) were set to reflect the absence of an energy barrier; and simulations using other values for these parameters showed that deposition fluxes were insensitive to the specific values of ζ_c and ζ_p when they yielded no energy barrier. The observed trend of increasing deposition flux with increasing fluid velocity (in the absence of an energy barrier to deposition) was well matched in the simulations (Figure 1). As well, the observed minimum deposition flux corresponding to the 1-μm diameter colloids was well-matched by the simulations (Figure 1), indicating that this minimum is explained by the interplay of diffusion, settling, and fluid drag forces as represented in the model. The relatively mild increase in deposition flux with increased fluid velocity observed for the 2.0-μm microspheres was also reflected in the simulated fluxes, again indicating that the influences of sedimentation, diffusion, and fluid drag forces

are reasonably represented in the model. Slight discrepancies between the observed and simulated values may reflect minor experimental inaccuracies (e.g., quantification of influent concentrations), as well as approximation of the flow field using a single parameter and minor inaccuracy in vendor-supplied concentrations. The ability of the simulations to capture overall trends with flow rate and colloid size is a strong indication that the model captured the essential processes governing deposition in the absence of an energy barrier.

Deposition Efficiency in the Presence of an Energy Barrier to Deposition. Deposition was observed for all four sizes of microspheres in the presence of a large energy barrier to deposition (Figure 2). The deposition efficiencies (the ratio of the deposition flux in the presence versus the absence of an energy barrier to deposition) decreased for all four sizes of , microspheres as a function of fluid velocity on glass and quartz substrata (Figure 2)**.** To put this in terms of deposition fluxes; the deposition flux increased less with increasing fluid velocity in the presence relative to the absence of an energy barrier to deposition. The 42 experiments represented in Figures 1 and 2 convincingly demonstrate the important influence of the energy barrier on colloid deposition under the conditions of the experiments. Specifically, the clear decrease in deposition efficiency with increasing fluid velocity (Figure 2) indicates a mitigating effect of fluid drag on colloid deposition in the presence of an energy barrier to deposition under these conditions. Notably, α decreased with fluid velocity similarly for all four sizes of microspheres. This trend was observed on both the glass and quartz substrata for the 0.5-, 1.0-, and 2.0-μm microspheres. Deposition on quartz substrata was not examined for the 0.2-μm microspheres, given the consistency of results between glass and quartz substrata observed for the other microsphere sizes. The observed decreases in α in this impinging jet system (0.005−0.02 day m^{-1}) were similar to those observed in porous media for an even larger range of colloid types, colloid sizes, and fluid velocities (0.0001−0.05 day m^{-1}) (*25*), suggesting that the mechanism mitigating deposition on the overall like-charged impinging surface may also operate (although not necessarily exclusively) in porous media.

Simulated deposition fluxes to a like-charged impinging surface ($\zeta_p = -60$ mV, $\zeta_c = -40$ mV) were zero under the experimental conditions, and this result was insensitive to variation in these parameters under all conditions where the resulting energy barrier was greater than several tens of kT. Therefore, the observed deposition onto glass and quartz in the presence of an energy barrier cannot be explained without the existence of local features that reduce or eliminate the energy barrier to deposition, as has been described in many other publications (e.g., *17*−*19*).

Discussion

Previously published numerical simulations demonstrate the potential for fluid drag to mitigate colloid deposition indirectly by decreasing colloid flux to the impinging surface. Prieve and Lin (*31*) and Yang et al. (*32*) simulated colloid deposition in impinging jet systems in the presence of a moderate energy barrier (<15 kT) and a deep secondary energy minimum (>5 kT). These simulations indicate that, under these restricted conditions, colloids accumulate within the secondary energy minimum outboard of the energy barrier, where they are subject to tangential fluid drag and are swept downstream, thereby decreasing the flux of colloids normal to the surface (i.e., over the energy barrier to the primary energy minimum) (*31*, *32*). This indirect mechanism of α mitigation is supported by our experimental observations, which show that mobile microspheres increasingly accumulated within the evanescent field (within ∼150 nm of the impinging surface) with increasing ionic strength.

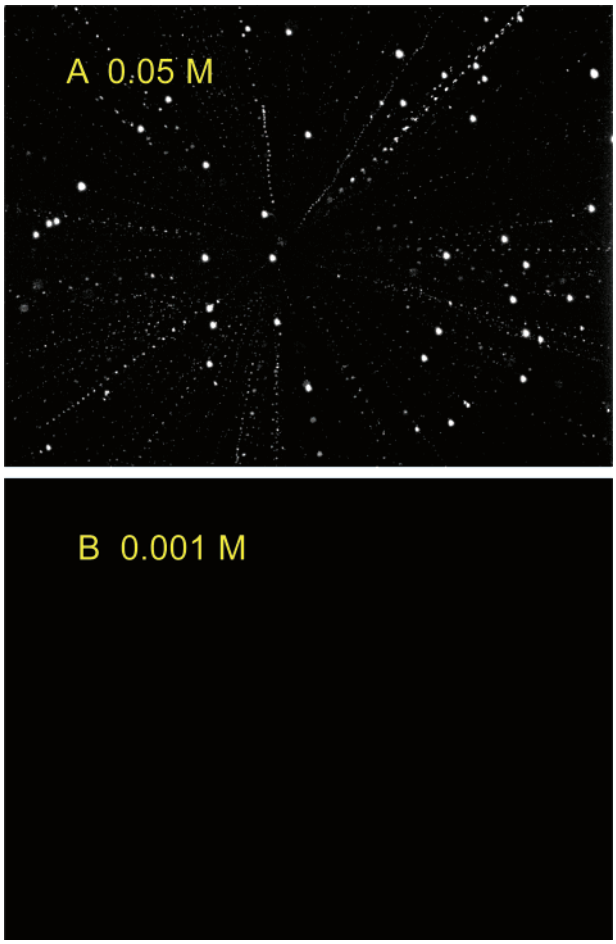

FIGURE 3. Images (10× magnification) of 1.0-μm microspheres captured during the first several minutes of injection at 1.06×10^{-3} m sec^{-1} at high ionic strength (0.05 M) (a) and at low ionic strength (0.001 M) (b). Visible streaks represent mobile particles at a separation distance within 150 nm of the surface.

Comparison of TIRFM images taken during the first several minutes of injection (prior to significant deposition) under equivalent fluid velocities show that the near-surface concentration of mobile microspheres was much greater at higher ionic strengths (deeper secondary energy minimum) (Figure 3a) relative to lower ionic strength (shallow or absent secondary energy minimum) (Figure 3b). The near-surface mobile microspheres were visible as streaks in the TIRFM images due to their movement during image acquisition (Figure 3a), whereas these mobile microspheres were absent under equivalent experimental and image acquisition conditions at low ionic strength (Figure 3b).

Although the above observations corroborate the simulations of Prieve and Lin (*31*) and Yang et al. (*32*), the fact that α was observed to decrease with increasing fluid velocity in a similar system at both low (0.006 M) and high (0.02 M) ionic strength (*26*) indicates that the mechanism of α decrease may be independent of the depth of the secondary energy minimum. Hence, other potential mechanisms driving the observed trend must also be considered.

Fluid drag may potentially mitigate colloid deposition via re-entrainment of colloids; however, negligible colloid re-entrainment occurred during injection and elution in the impinging jet system. Negligible re-entrainment occurred during elution even when the fluid velocity was increased by a factor of 200 following deposition, further suggesting that the colloids were associated with the surface via the primary energy minimum. The ability of the microspheres to "reach" the primary energy minimum despite the large energy barrier

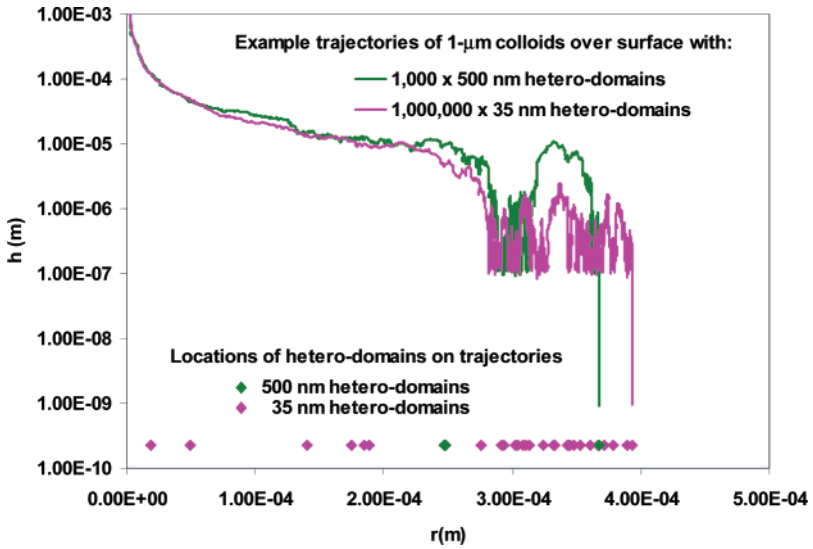

FIGURE 4. Example trajectories for a 1-μm colloid impinging surface with 1000 500-nm hetero-domains (green) and 1 000 000 35-nm hetero-domains (pink). Locations of the corresponding hetero-domains on the particle trajectories are also shown.

to deposition (indicated by measured surface characteristics) suggests that surface roughness or surface charge heterogeneity locally reduced or eliminated the energy barrier to deposition, and this possibility is corroborated by the reentrainment of (30−50%) of the attached microspheres upon introduction of high pH (11) solution to the impinging jet under the same velocity condition used for injection. The increased pH would be expected to reverse the charge on any positively charged domains on the impinging surface, thereby eliminating existing zones of attractive colloid−surface interaction.

Elimelech et al. (*33*) observed that microsphere deposition efficiencies decreased with increasing fluid velocity on an impinging micro-patterned charge-heterogeneous surface. The observation was interpreted to reflect interplay of hydrodynamic and electric double layer forces. Additionally, Nazemifard et al. (*34*) recently simulated colloid deposition onto a micro-patterned charge heterogeneous surface with stripes that were like- and opposite-charged to the colloid. Their simulations demonstrated that the fraction of opposite-charged surface available for deposition of the colloids decreased with increasing fluid velocity. These results suggest that the finite size of hetero domains responsible for colloid deposition onto overall like-charged surfaces may produce the observed decrease in α with increasing fluid velocity.

Below we present simulations of colloid deposition on bulk like-charged surfaces in order to demonstrate that deposition onto small favorable domains (hetero domains) can produce the observed decreases in α with increasing fluid velocity. Important differences between the valuable analysis provided by Nazemifard et al. (*34*) and this study include the fact that the former study examined a surface composed of alternating rings of opposite charge (bullseye), whereas this study examines the effect of hetero domains randomly distributed across a surface. Furthermore, Nazemifard et al. (*34*) did not include colloid diffusion in their model, which would alter the colloid trajectories and deposition fluxes, and they did not examine trends in colloid deposition efficiency versus fluid velocity, which is clearly a specific objective of this study.

Simulations using like-charged colloids and impinging surfaces ($\zeta_p = -60$ mV, $\zeta_c = -40$ mV) yielded deposition only when hetero domains were present on the surface. Example trajectories (1-μm colloid) at the low fluid velocity (Figure 4) are shown for a like-charged impinging surface with 1000 500-nm hetero domains or with 3 000 000 35-nm

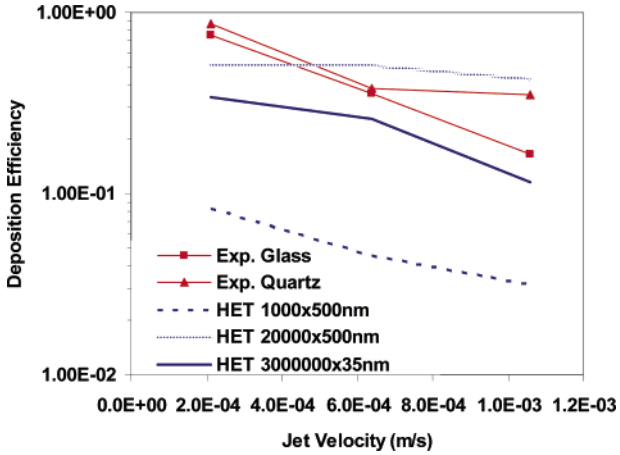

FIGURE 5. Deposition efficiencies (1-μm colloids) as a function of fluid velocity and the number of 500-nm hetero domains present on the impinging surface. The best fit was obtained for 3 000 000 35-nm hetero domains on the impinging surface.

hetero domains randomly distributed over the circular area below the jet (500-μm radius), comprising 0.01 and 1.4% coverage of the surface, respectively. The trajectories demonstrate that colloid diffusion toward the surface was repelled by the energy barrier except when the colloid was positioned over a hetero domain ($\zeta_c = +5$ mV). Many hetero domains were traversed, demonstrating the probabilistic nature of the deposition process, which requires diffusion toward the surface while over the hetero domain.

For 1.0-μm microspheres interacting with an overall like-charged substratum having 20 000 500-nm hetero domains (Figure 5), the simulated deposition efficiencies were constant with increasing fluid velocity, and so did not reflect the experimentally observed trends. However, decreasing the number of 500-nm hetero domains to 1000 produced decreases in α with increasing fluid velocity, yet the resulting simulated values of α were far below the observed values (Figure 5). Simulations using a larger number (3 000 000) of smaller-sized (35-nm) hetero domains produced decreases in α with increasing fluid velocity at values that approached those observed in the experiments. Therefore, given a sufficiently large number of sufficiently small hetero domains, both the trends and magnitudes of the deposition efficiency were well simulated. The same findings were qualitatively repeated for the other sizes of microspheres (Figure 2). We

cannot expect a quantitative match to the observed trends in the presence of an energy barrier to deposition due to the representational nature of the hetero domains and the use of generalized zeta potentials in these simulations. However, the ability of the simulations to capture general trends indicates that the observed decrease in α with increasing fluid velocity may be explained by the finite sizes of the hetero domains responsible for deposition.

It should be noted that the simulated trends in α do not result from under-representation of colloid translations across the hetero domains (i.e., due to too large a time step), as is explained in detail in the Supporting Information. The hetero domain is here represented as a hypothetical contiguous domain, whereas the physical mechanism may instead involve particular alignment of lattices of discreet charges on the colloid and collector surfaces (e.g., *35*, *36*). In either case, however, it is hypothesized that there is a finite domain over which colloid−surface repulsion is eliminated.

Acknowledgments

This material is based upon work supported by the National Science Foundation Hydrologic Sciences Program (EAR 0337258). Any opinions, findings, and conclusions or recommendations expressed in this material are those of the authors and do not necessarily reflect the views of the National Science Foundation. W.P.J. thanks Drs. Kirk Nelson and Tim Ginn for guidance and provision of the subroutine for conversion of uniform to Gaussian random number distribution. Drs. Tim Scheibe, Subir Bhattaharjee, Marshall Richmond, and Dennis Prieve provided helpful discussion during development of the model. We thank Dr. Charles Yang for assistance in developing the hydrodynamic retardation functions.

Supporting Information Available

Detailed description of experimental conditions and modeling. This material is available free of charge via the Internet at http://pubs.acs.org.

Literature Cited

(1) Yao, K. M.; Habibian, M. T.; O'Melia, C. R. Water and wastewater filtration: Concepts and applications. *Environ. Sci. Technol.* **1971**, *5* (11), 1105−1112.

(2) Rajagopalan, R.; Tien, C. Trajectory analysis of deep-bed filtration with the sphere-in-cell porous media model. *AIChE J.* **1976**, *22* (3), 523−533.

(3) Tufenkji, N.; Elimelech, M. Correlation equation for predicting single-collector efficiency in physicochemical filtration in saturated porous media. *Environ. Sci. Technol.* **2004**, *38*, 529−536.

(4) Nelson, K. E.; Ginn, T. R. Colloid filtration theory and the happel sphere-in-cell model revisited with direct numerical simulation of colloids. *Langmuir* **2005**, *21* (6), 2173−2184.

(5) Li, X.; Scheibe, T. D.; Johnson, W. P. Apparent decreases in colloid deposition rate coefficient with distance of transport under unfavorable deposition conditions: a general phenomenon. *Environ. Sci. Technol.* **2004**, *38* (21), 5616−5625.

(6) Li, X; Johnson, W. P. Nonmonotonic variations in deposition rate coefficients of microspheres in porous media under unfavorable deposition conditions. *Environ. Sci. Technol.* **2005**, *39* (6), 1658−1665.

(7) Li, X.; Zhang, P.; Lin, C. L.; Johnson, W. P. Role of hydrodynamic drag on microsphere deposition and re-entrainment in porous media under unfavorable conditions. *Environ. Sci. Technol.* **2005**, *39* (11), 4012−4020.

(8) Hamaker, H. C. The London-van der Waals attraction between spherical particles. *Physica* **1937**, *4*, 1058−1072.

(9) Lifshitz, E. M. The theory of molecular attractive force between solids. *Soviet Phys.* **1955**, *2* (1), 73−83.

(10) Russel, W. B.; Saville, D. A.; Schowalter, W. R. *Colloidal Dispersions*. Cambridge University Press: Cambridge, 1989.

(11) Israelachvili, J. N. *Intermolecular and Surface Forces,* 2nd ed.; Academic Press: London, 1992.

(12) Hogg, R.; Healy, T. W.; Fuerstenau, D. W. Mutual coagulation of colloidal dispersions. *Trans. Faraday Soc.* **1966**, *66*, 1638−1651.

(13) Wiese, G. R.; Healy, T. W. Effect of particle size on colloid stability. *Trans. Faraday Soc.* **1970**, *66*, 490.

(14) Nir, S. van der Waals interactions between surfaces of biological interest. *Prog. Surf. Sci* **1976**, *8*, 1−58.

(15) Gregory, J. Approximate expressions for retarded van der Waals interaction. *J. Colloid Interface Sci.* **1981**, *83*, 138−145.

(16) Elimelech, M.; Nagai, M.; Ko, C.-H.; Ryan, J. N. Relative insignificance of mineral grain zeta potential to colloid transport in geochemically heterogeneous porous media. *Environ. Sci. Technol.* **2000**, *34*, 2143−2148.

(17) Elimelech, M.; O'Melia, C. R. Kinetics of deposition of colloidal particles in porous media. *Environ. Sci. Technol.* **1990**, *24* (10), 1528−1536.

(18) Bhattacharjee, S.; Ko, C. H.; Elimelech, M. DLVO interaction between rough surfaces. *Langmuir* **1998**, *14*, 3365−3375.

(19) Shellenberger, K.; Logan, B. E. Effect of molecular scale roughness of glass beads on colloidal and bacterial deposition. *Environ. Sci. Technol.* **2002**, *36* (2), 184−189.

(20) Song, L.; Elimelech, M. Dynamics of colloid deposition in porous media: modeling the role of retained particles. *Colloids Surf., A* **1993**, *73*, 49−63.

(21) Song, L.; Elimelech, M. Transient deposition of colloidal particles in heterogeneous porous media. *J. Colloid Interface Sci.* **1994**, *167*, 301−313.

(22) Coston, J. A.; Fuller, C. C.; Davis, J. A. Pb^{2+} and Zn^{2+} adsorption by a natural aluminum- and iron-bearing surface coating on an aquifer sand. *Geochim. Cosmochim. Acta* **1995**, *59*, 3535−3547.

(23) Johnson, P. R.; Sun, N.; Elimelech, M. Colloid transport in geochemically heterogeneous porous media: Modeling and measurements. *Environ. Sci. Technol.* **1996**, *30* (11), 3284−3293.

(24) Zembala, M. Electrokinetics of heterogeneous interfaces. *Adv. Colloid Interface Sci.* **2004**, *112*, 59−92.

(25) Johnson, W. P.; Li, X.; Assemi, S. Hydrodynamic drag influences deposition and re-entrainment dynamics of microbes and nonbiological colloids during nonperturbed transport in porous media in the presence of an energy barrier to deposition. *Adv. Water Resour.* **2006**, in press.

(26) Brow, C.; Li, X.; Ricka, J.; Johnson, W. P. Comparison of microsphere deposition in porous media versus simple shear systems. *Colloids Surf., A* **2005**, *253*, 125−136.

(27) Kern, W.; Poutinen, D. Cleaning solutions based on hydrogen peroxide for use in silicon semiconductor technology. *RCA Rev.* **1970**, *31*, 187−206.

(28) Kuznar, Z. A.; Elimelech, M. Adhesion kinetics of viable *Cryptosporidium parvum* oocysts to quartz surfaces. *Environ. Sci. Technol.* **2004**, *38*, 6839−6846.

(29) Ohshima, H. Electrophoretic mobility of soft particles. *Colloids Surf., A* **1995**, *103*, 249−255.

(30) Gregory, J. Interaction of unequal double layers at constant change. *J. Colloid Interface Sci.* **1975**, *51*, 44−51.

(31) Prieve, D. C.; Lin, M. M. J. Adsorption of Brownian hydrosols onto a rotating disc aided by a uniform applied force. *J. Colloid Interface Sci.* **1979**, *76*, 32−47.

(32) Yang, C.; Dabros, T.; Li, D.; Czarnecki, J.; Masliyah, J. H. Kinetics of particle transport to a solid surface from an impinging jet under surface and external force fields. *J. Colloid Interface Sci.* **1998**, *208*, 226−240.

(33) Elimelech, M.; Chen, J. Y.; Kuznar, Z. A. Particle deposition onto solid surfaces with micropatterned charged heterogeneity: the "hydrodynamic bump" effect. *Langmuir* **2003**, *19*, 6594−6597.

(34) Nazemifard, N.; Masliyah, J. H.; Bhattacharjee, S. Particle deposition onto micropatterned charge heterogeneous substrates: trajectory analysis. *J. Colloid Interface Sci.* **2006**, *293*, 1−15.

(35) Holt, W. J. C.,; Chan, D. Y. C. Pair interactions between heterogeneous surfaces. *Langmuir* **1997**, *13*, 1577−1586.

(36) Khan, M. O.; Petris, S.; Chan, D. Y. C. The influence of discreet surface charges on the force between charged surfaces. *J. Chem. Phys.* **2005**, *122* (10), 104705−104712.

Received for review February 26, 2006. Revised manuscript received June 5, 2006. Accepted June 8, 2006.

ES060450C